Preparation and Slow-release Properties of Nanocellulose Composite Hydrogels

Kehong Zhang,[a,b,*] Xingyu Guo,[a] Yue Zhang,[a] Minyi Wang,[a] Wenqi Zhang [a]

Nanocellulose (CNF) was obtained from carrots using a combination of chemical treatment, mechanical milling, and ultrasonic treatment. Ultrafast preparation of maleic anhydride esterified nanocellulose was achieved by a hydrated hydrogen ion-driven dissociation, chemical cross-linking strategy based on a "one-pot" reaction method. Esterification modification with maleic anhydride reduced the crystallinity of nanocellulose and enhanced its thermal stability. High-strength drug-carrying hydrogels (MACNF/SA) with different drug loading capacities were prepared using cefixime (CFX) as a drug model and maleic anhydride esterified nanocellulose (MACNF) and sodium alginate (SA) as the main raw materials. The compressive strength of MACNF/SA hydrogels made from MACNF reached a maximum of 80.3 kPa when the mass ratio of CNF to MA was 2.5:12. Rheological property tests showed that the MACNF/SA hydrogels were pseudoplastic fluids with shear thinning. The drug release from the drug-carrying hydrogels followed non-Fickian diffusion.

DOI: 10.15376/biores.19.4.8976-8987

Keywords: Nanocellulose; Maleic anhydride; Sodium alginate; Hydrogel; Drug release

*Contact information: a: Anhui Engineering Research Center for Highly Functional Fiber Products for Automobiles, College of Materials and Chemistry, Anhui Agricultural University, Hefei, Anhui 230036, China; b: Fujian Provincial Key Lab of Coastal Basin Environment, Fujian Polytechnic Normal University, Fuqing, Fujian 350300 China; *Corresponding author: zkh@ahau.edu.cn*

INTRODUCTION

A hydrogel is a polymer with a three-dimensional network structure that is prepared through chemical or physical methods and can absorb a large amount of water and swell in the water due to its hydrophilic groups, such as -NH_2, -COOH, -OH, -$CONH_2$, -CONH, and -SO_3H (Olad *et al*. 2018; Kaczmarek *et al*. 2020; Cuéllar-Gaona *et al*. 2024). It can be flexible and soft as a result of its ability to absorb water. Chemical or physical cross-linking of natural or synthetic polymer chains can be used to design hydrogels. The mechanical properties, deformation behavior, and functional properties of hydrogels can be adjusted by changing the hydrophilic and hydrophobic ratios, the concentration of initiator or polymer, and the reaction conditions. Over the past 60 years, hydrogels have been engineered to be implantable, injectable, and paintable for many organs and tissues. In recent years, hydrogels have attracted great attention in soft robots, biomedicine, artificial muscles, drug delivery, wound dressings, and tissue engineering, and they have shown good application prospects. It is important to note that the design of most hydrogel actuators is inspired by organisms found in nature (Yang *et al*. 2024).

Biomass materials are materials derived from animals, plants, microorganisms, and other organisms in nature, which come from a rich variety of sources, mainly energy crops, agricultural wastes, wood and wood wastes, municipal solid wastes, aquatic plants, and

algae (Wang *et al*. 2023; Ibitoye *et al*. 2023; Zhang *et al*. 2023; Jiang *et al*. 2024). They are biodegradable, renewable, environmentally friendly, non-toxic, and are considered promising alternatives to petroleum-based products. Biomass materials are diverse, widely distributed, and abundant. Compared with synthetic polymers, biomass materials generally have better biodegradability. In the last two decades, research on natural hydrogels has focused on natural hydrogels, and there is a tendency to gradually replace synthetic hydrogels. Biopolymers have shown great potential, especially due to their large number of hydrophilic groups (hydroxyl and others). Biomass-based hydrogels are made from natural polymeric materials such as starch, cellulose, chitosan, sodium alginate and other natural polymeric materials with certain modifications based on certain physical and chemical cross-linking methods. Such hydrogels have shown a range of strength, biocompatibility, and biodegradability. Therefore, the preparation of functional hydrogels using biomass polymers has received extensive attention in recent years (Yang *et al*. 2024).

Cellulose is the basic structural component of plant cell walls and is the world's most abundant natural polymeric compound (Sundarraj and Ranganathan 2018). It possesses excellent functionality, biocompatibility, and low toxicity. The exposed polyhydroxy structure on its surface provides opportunities for modification and functionalization (Liyanage *et al*. 2021). Nanocellulose (CNF) has higher specific surface area and biodegradability, and exhibits nanoscale effects, excellent mechanical properties, strong hydrophilicity, and low thermal expansion (Thakur *et al*. 2021). The preparation of hydrogels from nanocellulose can improve water retention and absorption, salt resistance, and mechanical properties. As a result, there is increasing attention on the functionalized modification of nanocellulose and the preparation of its drug-loaded hydrogels. Li *et al*. (2024) developed a composite hydrogel SPBC by combining polyvinyl alcohol, sodium alginate, cellulose nanofibers, and sodium tetraborate decahydrate. The resulting SPBC has a range of excellent properties, including printability, conductivity, self-healing capabilities, and good mechanical strength. Its versatility and adaptability render it a prime candidate for applications in wearable devices and human motion monitoring. Ma *et al*. (2023) prepared an intricate interpenetrating network hydrogel using an acetic acid coagulation bath and Ca^{2+} chelation, taking advantage of the compatibility of CNF and sodium alginate (SA). This hydrogel, which has a high pH sensitivity, emerges as a suitable carrier for the sustained release of aspirin. Khalilzadeh *et al*. (2020) synthesized hydrogels through the copolymerization of CNF with acrylamide, utilizing acrylic acid (AA) and acrylamide (AM) as monomers and N,N-methylenebisacrylamide (MBA) as a crosslinking agent. These findings indicated that the reaction between CNF and the monomers is thermodynamically favorable, exhibiting a decreasing trend in the order of AM, AA, and MBA. This significant contribution facilitates the efficient production of renewable bioproducts derived from nanocellulose structures.

With around 40 million tons of carrots produced worldwide in 2023, carrot pomace left over from juice extraction (accounting for up to 30% to 50 % of the initial carrot mass) is an attractive alternative to wood pulp as a starting material for CNF production. The energy required to produce nanocellulose from carrots is significantly lower than that required to produce CNF from wood fibers. Additionally, carrot-derived nanocellulose possesses comparable or superior qualities to those originating from wood. Consequently, the preparation of cellulose nanofibrillated cellulose from carrots using a combination of chemical treatment, mechanical milling, and ultrasonic treatment is an important way to achieve high value utilization of carrots (Amoroso *et al*. 2021). Ultrafast preparation of maleic anhydride esterified nanocellulose can be achieved by a hydrated hydrogen ion-

driven dissociation-chemical cross-linking strategy based on a "one-pot" reaction method. Through adjusting the ratio of nanocellulose to maleic anhydride, nanocellulose with different degrees of esterification can be prepared. Mixing the esterified-CNF with sodium alginate can produce high-strength drug-carrying hydrogels, which is important for expanding the applications of nanocellulose.

EXPERIMENTAL

Materials

Carrots were supplied from a local vegetable market vendor (Hefei, China) and used as received. Sodium hydroxide (NaOH), sodium chlorite ($NaClO_2$), acetic acid (CH_3COOH), and maleic anhydride ($C_4H_2O_3$) were provided by Shanghai Aladdin Biochemical Technology Co., Ltd. (Shanghai, China) and used as received. Concentrated sulfuric acid (H_2SO_4), sodium alginate ($C_6H_9NaO_7$), and calcium chloride ($CaCl_2$) were purchased from Xilong Scientific Co., Ltd. (Shantou, China). Cefixime was provided by the United Laboratories International Holdings Limited (Zhuhai, China).

Preparation of the Sample

The grated carrots were dispersed in a 20% NaOH solution with a mass ratio of 2 wt%, subjected to magnetic stirring for 2 h at 80 °C, and subsequently washed to neutrality. A bleaching solution was prepared by mixing 10% acetic acid solution, 2 wt% sodium chlorite solution, and deionized water in a volume ratio of 1:1:1. The treated carrot residue was dispersed in the bleaching solution at a mass ratio of 2 wt%, stirred at 80 °C for 2 h, and then washed to neutral. The bleached carrot residue was processed with the UH-12 plant cellulose nano-grinder (Union-Biotech Co., Ltd., Shanghai, China) with high pressure homogenization for 10 min, and the translucent nanocellulose solution was obtained. The nanocellulose solution was freeze-dried at -90 ℃ in the SP freeze-dryer (Tegent Technology Co., Ltd., Hongkong, China) to produce CNF. According to the mass ratio of CNF to maleic anhydride of 1.5:12, 2.5:12, 3.5:12, 4.5:12, respectively, the nanocellulose was placed in a 20 wt% maleic anhydride solution and mixed evenly. Then, the 98 wt% sulfuric acid was slowly added dropwise at room temperature while stirring until the CNF was completely dissolved. The cellulose was washed by repeated centrifugation with ethanol and deionized water in the H2-16K high-speed centrifuge (Hunan Kecheng Instrument and Equipment Co., Ltd., Changsha, China) until the solution was neutral, and the centrifugation speed used was 8000 r/min. Four types of maleic anhydride esterified nanocellulose (MACNF) with different degrees of esterification were produced, which were denoted as MACNF-1, MACNF-2, MACNF-3, and MACNF-4, respectively. A certain amount of MACNF was weighed and dried to form a film to be used for the relevant property testing. Subsequently, an aqueous solution of MACNF with a concentration of 2 wt% was prepared by dispersing MACNF in deionized water and followed by ultrasonication at 1000 W for 30 min in the XM-1000T ultrasonic disperser (Xiaomei ultrasonic instrument Co., Ltd, Kunshan, China). The MACNF/SA mixed solution was prepared by mixing 2 wt% SA solution and 2 wt% MACNF solution according to the mass ratio of MACNF to SA of 2:1 and stirring at 50 °C for 1 h. Then, the cefixime was added to the MACNF/SA mixed solution at 0.5 wt%, 1.0 wt%, 1.5 wt% and 2 wt% drug-loading amounts, and poured into the mold after stirring at room temperature for 30 min. After cross-linking with 3 wt% calcium chloride solution for 1 h, the residual

calcium chloride solution on the surface of the drug-loaded hydrogel was rinsed off with deionized water. Four types of nanocellulose drug-loaded hydrogels were obtained, which were recorded as CFX/MACNF/SA-0.5, CFX/MACNF/SA-1, CFX/MACNF/SA-1.5, and CFX/MACNF/SA-2, respectively.

Characterization of the Sample

The chemical structures of all samples were tested using a TENSOR II infrared spectrometer (Bruker Corporation, Karlsruhe, Germany) in the range of 400 to 4000 cm^{-1} with a resolution of 4 cm^{-1}. The crystallinity of the samples was obtained using an XD-6 X-ray diffractometer (Beijing Puxi General Instrument Co., Ltd., Beijing, China) scanned in steps of 0.1 °/s in the range of 5° to 60°.

The compressive strength of hydrogel samples MACNF-1, MACNF-2, MACNF-3, and MACNF-4 was measured using an ETM520C universal testing machine (Shenzhen Wance Testing Machine Co., Ltd., Shenzhen, China) with the compression speed of 2 mm /min and the compressive strain of 50%. The test samples used were cylinders with a diameter of 120 mm and a height of 60 mm. The results of mechanical properties were an average of results from 5 samples.

The rheological properties of the hydrogel samples were measured by a RVDV-III rotary rheometer (Thermo Fisher Scientific, Waltham, MA, USA). The test samples used were cylinders with a height of 2 mm and a diameter of 2 mm. The thermal stability of the samples was measured at a heating rate of 10 °C/min in the range of 50 to 600 °C using a thermogravimetric (TGA)/differential scanning calorimetry (DSC) 1/1100 thermal analyzer (Mettler-Toledo International Inc., Zurich, Switzerland) under nitrogen protection. To analyze the drug release behavior of the gels with different drug loading capacities, the drug loaded aqueous gels were immersed in 30 mL of deionized water. The drug concentration during extended release was measured by taking 2 mL of the mixed solution every 10 min using a pipette gun. The absorbance of the solution at a wavelength of 288 nm was determined using an UV/V-16/18 UV–vis spectrophotometer (Shanghai Yiheng Scientific Instrument Co., Ltd, Shanghai, China) to determine the concentration of cefixime. All the drug release experiments were repeated twice. The morphologies of wood and transparent wood samples were analyzed using a Hitachi S-4800 scanning electron microscope (SEM) (Hitachi, Ltd., Tokyo, Japan) at an accelerating voltage of 3.0 kV.

RESULTS AND DISCUSSION

FTIR Analysis

Figure 1 shows the FTIR spectra of CNF, SA, esterification-modified CNF (MACNF), and MACNF/SA. The broad peaks in the range of 3700 to 3100 cm^{-1} belong to intramolecular and intermolecular -OH stretching vibrations. Typical characteristic peaks of nanocellulose include 2900 cm^{-1} for C-H stretching vibration absorbance, 1373 cm^{-1} for C-H bending vibration absorption, and 1060 cm^{-1} for C-O stretching vibration. In the FTIR spectra of esterified CNF (MACNF), the characteristic peak at 1735 cm^{-1} is the C=O stretching vibration absorbance peak, the characteristic peak at 1426 cm^{-1} is the absorbance peak caused by the asymmetric stretching vibration of C=O, the characteristic peak at 1630 cm^{-1} is the C-O bending vibration absorbance peak, and the characteristic peak located at 1093 cm^{-1} is the C-O stretching vibration absorbance peak. The presence of these absorbance peaks indicates that MA undergoes a chemical reaction with CNF as shown in

Fig. 2. The intensity of the stretching vibration peaks of C=O increases with increasing MA content, which is attributed to the fact that the increase in the maleic anhydride content in the mixed acid drives the esterification of the product. This may be due to the degradation reaction of cellulose under the effect of higher concentration of sulfuric acid, which destroyed the structure of cellulose and reduced the effective reaction site, leading to the decrease of esterification. Comparative analysis reveals that the hydroxyl peak position in the FTIR spectra of the MACNF/SA hydrogel is shifted, indicating that the interaction between SA and MACNF is not a simple physical mixing.

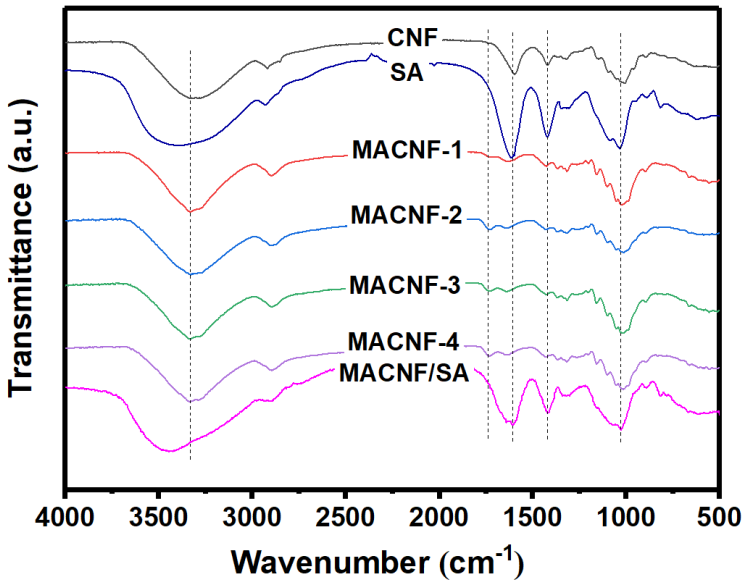

Fig. 1. FTIR spectra of CNF, SA, esterification-modified CNF (MACNF) and MACNF/SA

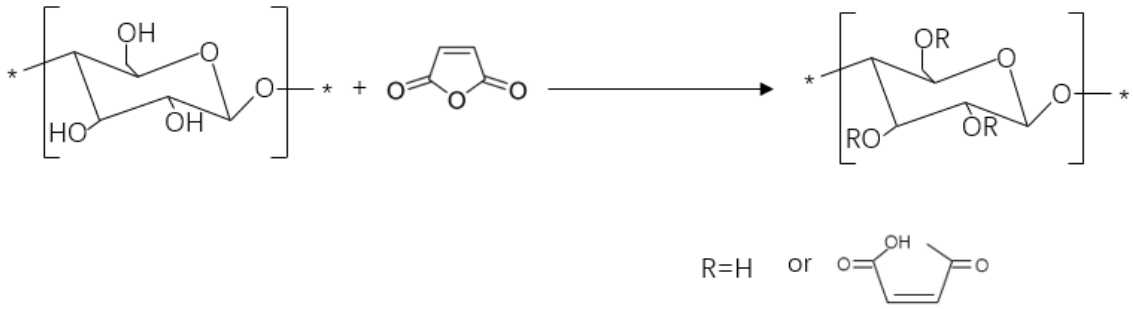

Fig. 2. Reaction mechanism of MA and CNF

X-ray Diffraction (XRD) Analysis

The XRD patterns of CNF and esterified CNF are shown in Fig. 3. The diffractograms displayed the typical cellulose-I crystal structure of CNF with 2θ diffraction peaks located at 14.8°, 16.4°, and 22.6° corresponding to the (101), (110), and (200) crystallographic planes, respectively. The 2θ diffraction peaks of the esterified CNF appeared at 15.8° and 22.8°, corresponding to crystal planes (101) and (020), respectively, still showing cellulose-I crystal structure. This indicates that the cellulose in CNF had not been completely dissolved in the course of esterification. After esterification with maleic anhydride, the crystallinity of CNF decreased from 68.0% to 56.9%. This can be attributed

to many H^+ ions having broken the hydrogen bonds between cellulose molecules inside CNF during the esterification reaction, resulting in the destruction of some of the order of the crystallization zone.

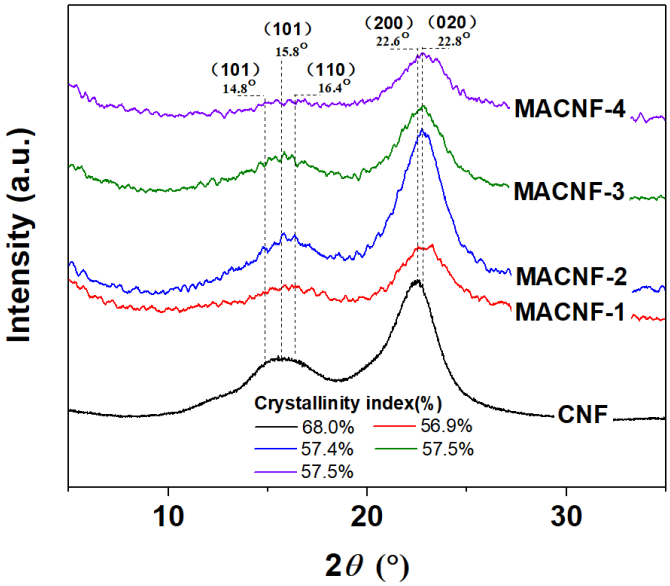

Fig. 3. XRD patterns of CNF and MACNF with different degrees of esterification

TG Analysis

The thermal behaviors of CNF, MACNF-1, MACNF-2, MACNF-3, and MACNF-4 in the nitrogen atmosphere were investigated. The weight loss of the samples at different temperatures was recorded and analyzed to characterize the thermal stabilities of the samples in the temperature range of 50 to 600 °C. As shown in Fig. 4, CNF underwent rapid thermal degradation in the temperature range of 250 to 360 °C.

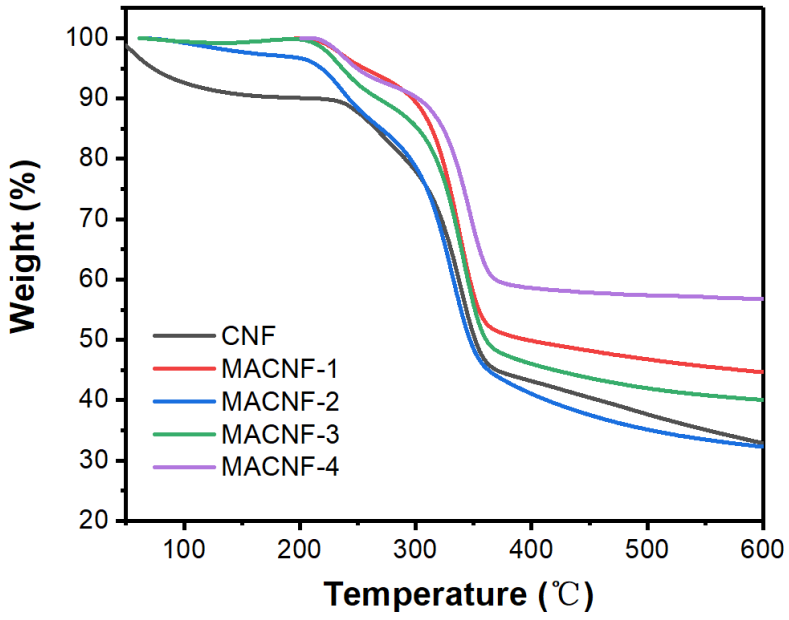

Fig. 4. TG curves of CNF and MACNF with different degrees of esterification

The onset temperature of rapid thermal degradation of CNF modified by MA increased, indicating that esterification increased the thermal stability of CNF. The residual carbon rate of esterified CNF at 600 °C decreased with increasing degree of esterification. The low thermal stability of maleic anhydride leads to the decomposition of the new groups introduced into CNF at lower temperatures, resulting in lower thermal stability after esterification.

Mechanical Property Analysis

The degree of esterification influenced the compressive strength of MACNF/SA hydrogels. As shown in Fig. 5, the compressive strengths of MACNF/SA hydrogels showed an increase and then a decrease with the decrease of esterification degree. When the mass ratio of CNF to MA was 2.5:12 (sample MACNF-2), the compressive strength of the hydrogel reached a maximum of 80.33 kPa. This was due to the hydrolysis of CNF cellulose caused by the increase in the amount of mixed acid, which reduced the degree of cellulose polymerization and decreased the mechanical strength of MACNF/SA hydrogel.

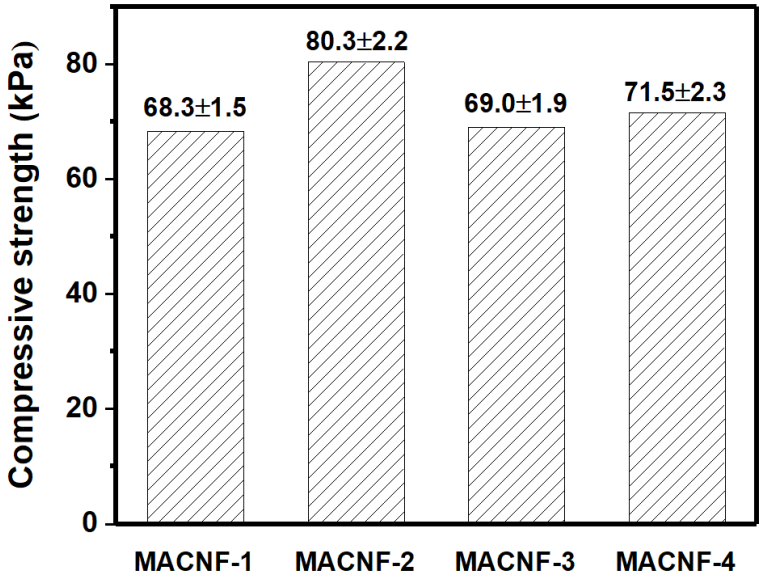

Fig. 5. Compression curves of MACNF/SA hydrogel with different degrees of esterification (the compressive strain of 50%)

SEM Analysis

In order to clearly see the morphology of CNF and CFX/MACNF/SA hydrogel prepared from carrots, the cellulose nanofibers and CFX/MACNF/SA hydrogel were characterized by field emission scanning electron microscopy after freeze-drying. The internal structure of CNF and the surface structure of CFX/MACNF/SA hydrogel are shown in Fig. 6. As can be seen from Fig. 6(a), the CNF exhibits stacked interwoven states, forming a three-dimensional network structure. The cellulose nanofibers were linked together due to hydrogen bonding to form a strong nano-network. The diameters of CNF were mostly distributed between 10 and 30 nm. Due to the small diameter and uniform distribution of CNF, the aspect ratio is large, and the specific surface area was large, which endows the CNF with excellent mechanical properties after formation into a structure. The CNF was uniformly distributed on the surface of CFX/MACNF/SA hydrogel, as shown in Fig. 6(b). Under the action of ionic cross-linking agent and the support of CNF, SA formed

a thin film-like structure between CNF. The CNF intertwined with each other and played a good role in fixing and supporting the internal SA, which made the CFX/MACNF/SA hydrogel present a composite cross-linked structure consisting of SA and CNF interpenetrating cross-linking. This continuous and stable porous structure can effectively increase the specific surface area of the hydrogel material, thus enhancing the diffusion interaction between the hydrogel system and the surrounding solution.

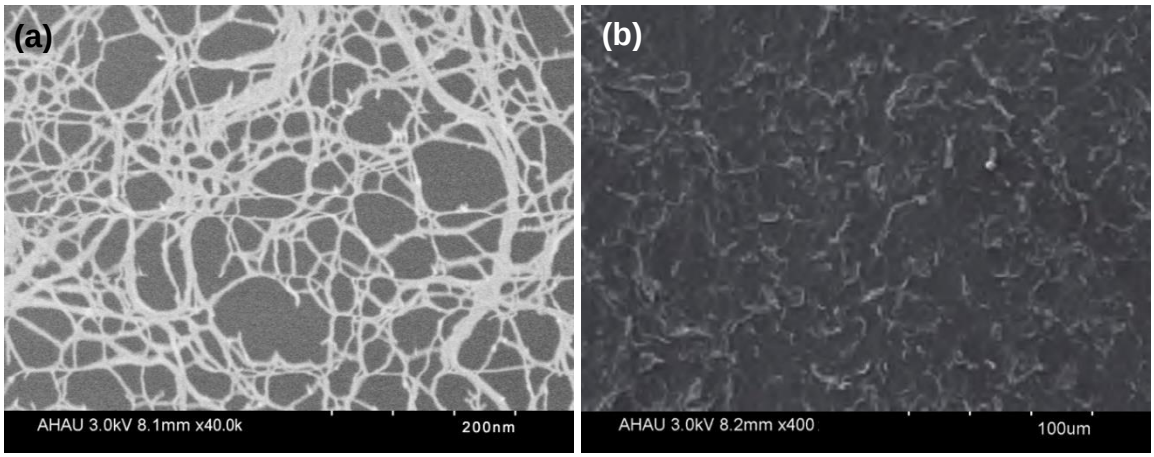

Fig. 6. SEM images of (a) CNF, and (b) CFX/MACNF/SA drug-loaded hydrogels

Rheological Property Analysis

The rheological curves of the hydrogels (denoted as MACNF/SA) produced by blending SA with MACNF of various esterification degrees are shown in Fig. 7. It can be seen that the viscosity of MACNF/SA hydrogels at lower shear rates decreased rapidly with the increase of shear rate. The viscosity of the hydrogels prepared by MACNF-1 and MACNF-3 decreased less rapidly than those of the hydrogels prepared by MACNF-2 and MACNF-4. The slower decrease in viscosity with increasing shear rate indicates that the prepared MACNF/SA hydrogels were pseudoplastic fluids with shear-thinning properties.

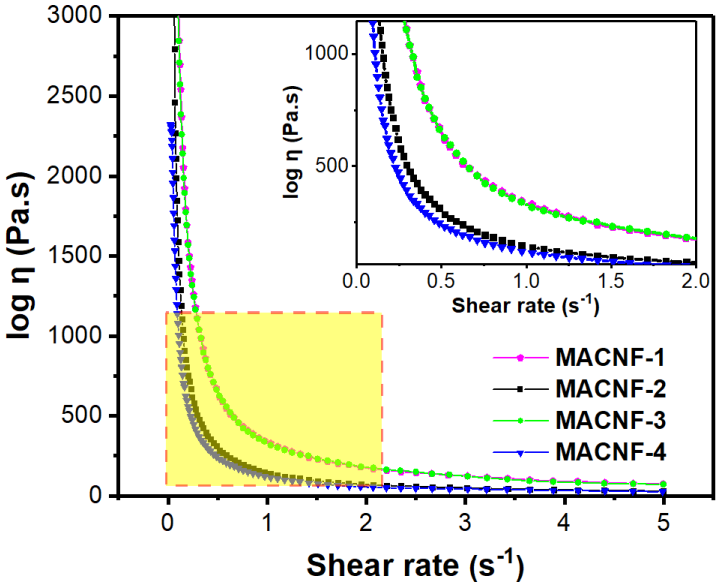

Fig. 7. Rheological properties of MACNF/SA hydrogels with different degrees of esterification

Analysis of Hydrogel Release Properties

Figure 8 shows the *in vitro* release curve of drug-loaded MACNF/SA hydrogels. For the release behavior of hydrogels with different drug loading amounts, the curves in Fig. 8(a) shows that the release rate of CFX was faster within 120 min. There was little difference in drug release between hydrogel samples with drug loading greater than 1%. The degree of esterification had a significant effect on the drug release behavior of the hydrogels. The drug release behavior of hydrogel samples in Fig. 8(b) indicates that the increase in the degree of esterification of MACNF decreased the release rate of CFX. The increase in the degree of esterification elevated the affinity of the hydrogel for the drug, causing a decrease in the drug release rate. To investigate the release mechanism of CFX/MACNF/SA hydrogel, the Korsmeyer-Peppas model was used to fit the CFX release and analyze the cumulative drug release kinetics (Askarizadeh *et al*. 2023). In the model $M_t/M_\infty = at^n$, M_t is the cumulative release at time t, M_∞ is the maximum drug release throughout the release process, t is the drug release time, and a and n are the release constant and release index. The fitting curves of drug release behavior of CFX/MACNF/SA hydrogels with different drug loadings are shown in Fig. 9. The R^2 values were all greater than 0.9, indicating that the release process of CFX in CFX/MACNF/SA hydrogels was more consistent with the Korsmeyer-Peppas model. The values of n in the models were between 0.45 and 0.89, indicating that the release behavior of CFX in CFX/MACNF/SA hydrogels was non-Fickian diffusion, and the drug was released through dissolution, diffusion, and matrix erosion.

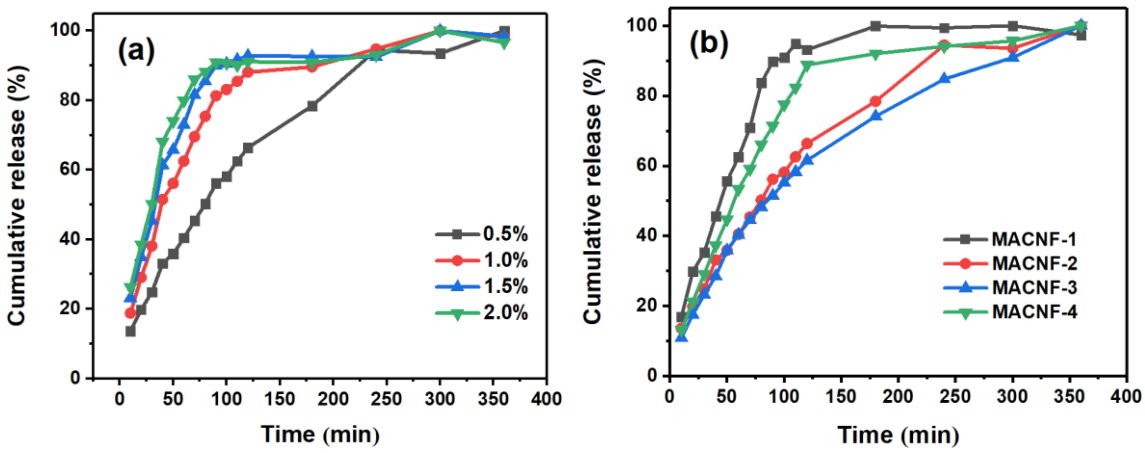

Fig. 8. Cumulative release curves of CFX/MACNF/SA drug-loaded hydrogels: (a) MACNF-2/SA hydrogels with different drug loading amounts; (b) MACNF with different degrees of esterification

In this study, a new route for the targeted synthesis of maleic anhydride esterified nanocelluloses (MACNCs) from carrots was developed based on the principle of "one-pot reaction" without separation of intermediates and without organic solvent. It provides a new path for the efficient and green functional modification of nanocellulose. Nanocellulose has excellent bioactivity, low toxicity, biocompatibility, biodegradability and excellent mechanical properties. The design and construction of novel nanocellulose drug carriers can not only achieve targeted drug delivery, but also play a role in regulating the drug release rate, which is expected to expand the application of nanocellulose in drug sustained and controlled release systems.

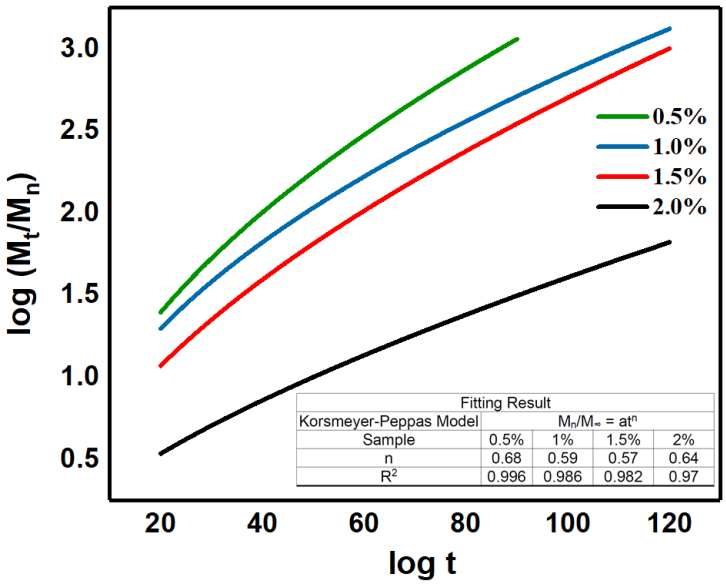

Fig. 9. Fitting curves of CFX/MACNF/SA drug-loaded hydrogels with different drug loading amounts

CONCLUSIONS

1. Nanocellulose was prepared from carrot by high pressure homogenization and ultrasonic treatment. Maleic anhydride esterified CNF was prepared by hydrated hydrogen ion driven dissociation-chemical cross-linking strategy. The thermal stability of nanocellulose was effectively improved.
2. High-strength drug-carrying hydrogels with different drug loading capacities were produced by blending sodium alginate and MACNF using cefixime as a drug model. Rheological property tests showed that the MACNF/SA hydrogels were pseudoplastic fluids with shear-thinning properties. The compressive strength of the prepared MACNF/SA hydrogels was maximized when the mass ratio of CNF to MA was 2.5:12.
3. The results of the sustained-release test showed that the MACNF hydrogel had a good sustained-release effect on drugs. The release behavior of the MACNF/SA drug-carrying hydrogel conformed to the Peppas model for non-Fickian diffusion.

ACKNOWLEDGMENTS

The authors are grateful for the support of the Natural Science Research Project of Anhui Educational Committee, Grant No. 2023AH050979; the Open Fund of Fujian Provincial Key Lab of Coastal Basin Environment, Grant No. S1-KF2003; the Anhui Agricultural University - Anhui Huayi Packaging Technology Co., Ltd. cooperation project, Grant No. hx23402; and Anhui Agricultural University College Students Innovation and Entrepreneurship Training Program, Grant Nos. S202210364147, S202310364142, and S202310364153.

REFERENCES CITED

Amoroso, L., De France, K. J., Milz, C. I., Siqueira, G., Zimmermann, T., and Nystrom, G. (2021). "Sustainable cellulose nanofiber films from carrot pomace as sprayable coatings for food packaging applications," *ACS Sustainable Chemistry and Engineering* 10(1), 342-352. DOI: 10.1021/acssuschemeng.1c06345

Askarizadeh, M., Esfandiari, N., Honarvar, B., Sajadian, S. A., and Azdarpour, A. (2023). "Kinetic modeling to explain the release of medicine from drug delivery systems," *ChemBioEng Reviews* 10(6), 1006-1049. DOI: 10.1002/cben.202300027

Cuéllar-Gaona, C. G., González-López, J. A., Martínez-Ruiz, E. O., Acuña-Vazquez, P., Dávila-Medina, M. D., Cedillo-Portillo, J. J., Narro-Céspedes, R. I., Soria-Arguello, G., Puca-Pacheco, M., Ibarra-Alonso, M. C., and Neira-Velázquez, M. G. (2024). "Chitosan hydrogels with antibacterial and antifungal properties: enhanced properties by incorporating of plasma activated water," *Plasma Chemistry and Plasma Processing*, 1-20. DOI: 10.1007/s11090-024-10506-3

Ibitoye, S. E., Mahamood, R. M., Jen, T. C., Loha, C., and Akinlabi, E. T. (2023). "An overview of biomass solid fuels: Biomass sources, processing methods, and morphological and microstructural properties," *Journal of Bioresources and Bioproducts* 8(4), 333-360. DOI: 10.1016/j.jobab.2023.09.005

Jiang, S., Liu, H., Zhang, W., Lu, Y. (2024). "Bioanode boosts efficacy of chlorobenzenes-powered microbial fuel cell: Performance, kinetics, and mechanism," *Bioresource Technology* 405, 130936. DOI: 10.1016/j.biortech.2024.130936

Kaczmarek, B., Nadolna, K., and Owczarek, A. (2020). "The physical and chemical properties of hydrogels based on natural polymers," in: *Hydrogels Based on Natural Polymers*, Elsevier, Amsterdam, Netherlands, pp. 151-172. DOI: 10.1016/B978-0-12-816421-1.00006-9

Khalilzadeh, M. A., Hosseini, S., Rad, A. S., and Venditti, R. A. (2020). "Synthesis of grafted nanofibrillated cellulose-based hydrogel and study of its thermodynamic, kinetic, and electronic properties," *Journal of Agricultural and Food Chemistry* 68(32), 8710-8719. DOI: 10.1021/acs.jafc.0c03500

Li, M., Wang, Y., Wei, Q., Zhang, J., Chen, X., and An, Y. (2024). "A high-stretching, rapid-self-healing, and printable composite hydrogel based on poly (vinyl alcohol), nanocellulose, and sodium alginate," *Gels* 10(4), article 258. DOI: 10.3390/gels10040258

Liyanage, S., Acharya, S., Parajuli, P., Shamshina, J. L., and Abidi, N. (2021). "Production and surface modification of cellulose bioproducts," *Polymers* 13(19), article 3433. DOI: 10.3390/polym13193433

Ma, H., Zhao, J., Liu, Y., Liu, L., Yu, J., and Fan, Y. (2023). "Controlled delivery of aspirin from nanocellulose-sodium alginate interpenetrating network hydrogels," *Industrial Crops and Products* 192, article ID 116081. DOI: 10.1016/j.indcrop.2022.116081

Olad, A., Pourkhiyabi, M., Gharekhani, H., and Doustdar, F. (2018). "Semi-IPN superabsorbent nanocomposite based on sodium alginate and montmorillonite: Reaction parameters and swelling characteristics," *Carbohydrate Polymers* 190, 295-306. DOI: 10.1016/j.carbpol.2018.02.088

Sundarraj, A. A., and Ranganathan, T. V. (2018). "A review on cellulose and its utilization from agro-industrial waste," *Drug Invention Today* 10(1), 89-94.

Thakur, V., Guleria, A., Kumar, S., Sharma, S., and Singh, K. (2021). "Recent advances in nanocellulose processing, functionalization and applications: A review," *Materials Advances* 2(6), 1872-1895. DOI: 10.1039/D1MA00049G

Wang, Y., Xu, T., Liu, K., Zhang, M., Cai, X. M., and Si, C. (2023). "Biomass-based materials for advanced supercapacitor: Principles, progress, and perspectives," *Aggregate* 5(1), article e428. DOI:10.1002/agt2.428

Yang, M, Liu Y, Duan G, Liang, Z., Huang, Y., Zhang, C., Han, X. S., Ma, C. X., He, S. J., and Jiang, S. H. (2024). "Recent advances of biomass-based smart hydrogel Actuators: A review," *Chemical Engineering Journal*, article 155157. DOI: 10.1016/j.cej.2024.155157

Zhang, Y., Xiao, H., Xiong, R., and Huang, C. (2023). "Xylan-based ratiometric fluorescence carbon dots composite with delignified wood for highly efficient water purification and photothermal conversion," *Separation and Purification Technology* 324, article 124513. DOI: 10.1016/j.seppur.2023.124513

Article submitted: July 13, 2024; Peer review completed: August 17, 2024; Revised version received: September 23, 2024; Accepted: September 24, 2024; Published: October 10, 2024.
DOI: 10.15376/biores.19.4.8976-8987